

Polar Geomagnetic Disturbances and Auroral Substorms During the Magnetic Storm on 20 April 2020

Gromova L.I.¹, Kleimenova N.G.², Despirak I.V.³, Gromov S.V.¹, Lubchich A.A.³,
Malysheva L.M.²

¹Pushkov Institute of Terrestrial Magnetism, Ionosphere, and Radio Wave Propagation, Moscow,
Troitsk, Russia; e-mail: ligromova@yandex.ru

²Schmidt Institute Physics of the Earth RAS, Moscow, Russia

³Polar Geomagnetic Institute, Apatity, Russia

Abstract

The global features of the spatial-temporal distribution of high-latitude geomagnetic disturbances have been studied during the first magnetic storm (20 April 2020) of the new, 25-th cycle of the solar activity. Basing on the ground-based measurements by the global networks SuperMAG, INTERMAGNET and IMAGE magnetometers, it was shown that the geomagnetic disturbances during this storm was significant ($Kp = 5$) despite the low speed of the magnetic cloud (MC) that caused this storm. So, in the storm initial phase, there was developed the high-latitude geomagnetic disturbances which were concentrated at the morning-dayside polar latitudes above $\sim 65\text{-}70^\circ$ Mlat. It was found the high-latitude vortices of the geomagnetic field which could indicate the local intensification of the Field-Aligned Currents. Two intense (> 1000 nT) auroral substorms were observed in the storm-main phase, caused by an appearance of large amplitudes of the southward IMF B_z . Thus, the magnetic storm geoeffectiveness depends more on the appearance of large values of the southward IMF than on the low values of the solar wind speed.

Keywords: magnetic cloud, magnetic storm, geomagnetic disturbances

1. Introduction

The storm on 20 April 2020 was the first magnetic storm of the new 25 solar cycle. It developed after the long period of the quiet solar wind and, correspondingly, weak geomagnetic activity ($Kp \leq 2$) that it is shown in Figure 1. The storm was associated with a *slow* magnetic cloud (MC) approached the magnetosphere of the Earth. The detailed overview of the solar event caused this MC and, as a result, the considered magnetic storm, was reported in [Davies et al., 2021; O’Kane et al., 2021].

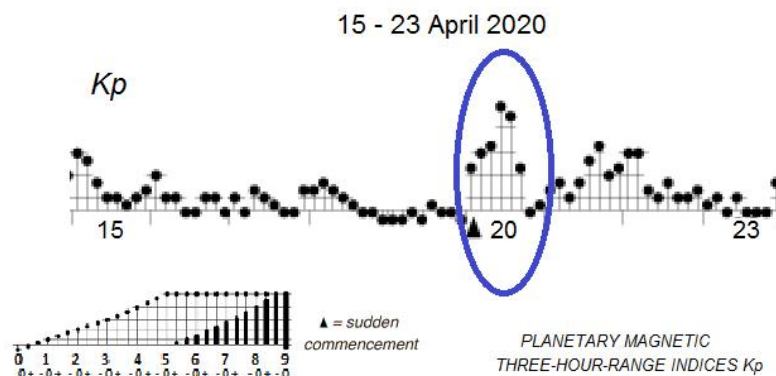


Figure 1. Planetary geomagnetic index Kp before and during the magnetic storm on 20 April 2020. After <https://wdc.kugi.kyoto-u.ac.jp/kp/>

Usually, geoeffectiveness of slow magnetic clouds is low, they do not cause intense storms [Richardson and Cane, 2012]. There are lot of works studying intense magnetic storms caused by *fast* magnetic clouds, e.g., [Tsurutani et al. 1992, Kleimenova et al. 2021 and references therein]. But magnetic storms associated with *slow* magnetic clouds have not been studied enough, e.g., [Nitta et al, 2021], as well as their high-latitude geomagnetic effects.

The aim of our paper is to study high-latitude geomagnetic disturbances during the magnetic storm of 20 April 2020 as a storm associated with the slow solar wind.

2. Space weather on 20 April 2020

The variations of the interplanetary magnetic field (IMF) and solar wind parameters on 20 April 2020 are shown in Figure 2. One can see that the magnetic cloud approached the Earth

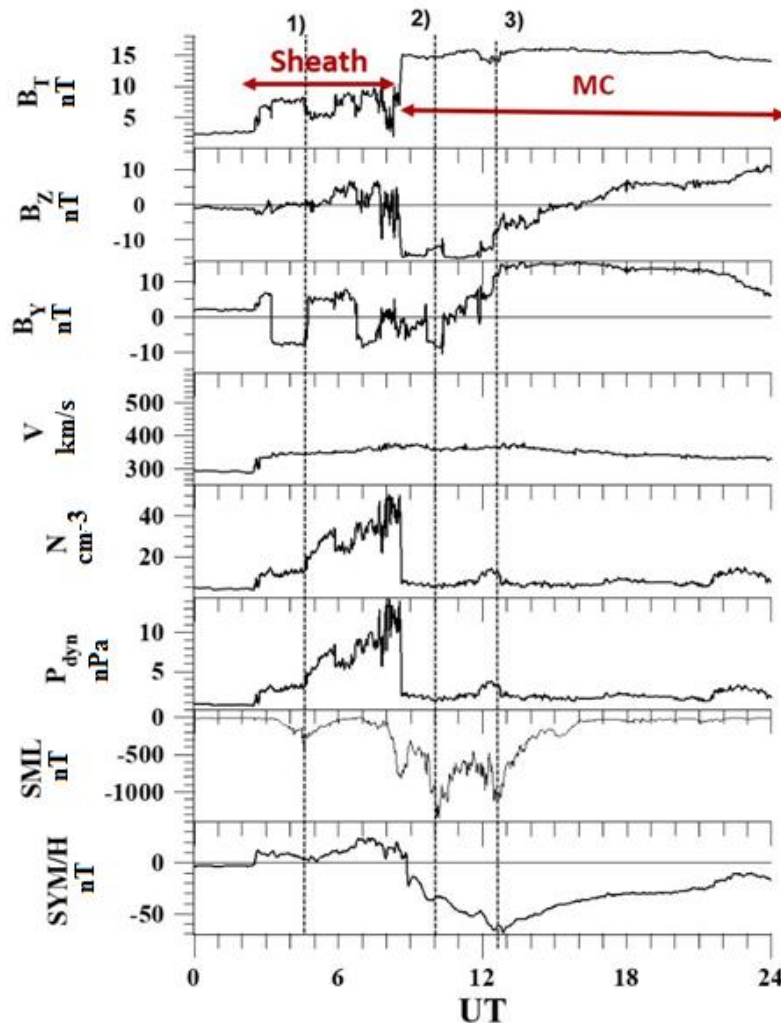


Figure 2. The variation of the IMF and solar wind parameters, planetary indices SML-index of the auroral activity and SYM/H-index of the storm The red horizontal arrows show the boundary of the large-scale streams of the solar wind (SHEATH and MC). Data from <http://omniweb.gsfc.nasa.gov> and <http://supermag.jhuapl.edu/mag>.

with the low speed of the solar wind. The magnetic cloud was characterized by a low and practically unchanged speed of the solar wind, but with a significant amplitude of the southward Interplanetary Magnetic Field (B_z IMF reached -15 nT), which was not changed for about 4 hours. Apparently, this led to the development of a moderate magnetic storm with a maximum value of SYM/H \sim -70 nT. The low solar wind speed (\sim 350-400 km/s) which did not change during the storm makes it possible, on the one hand, to reveal geomagnetic disturbances that

are not related to the solar wind speed, and, on the other hand, to consider the influence of the IMF components on them. Here we used *SYM/H*-index as 1-min analog of the 1-hour *Dst*-index, and *SML*-index of the auroral activity that shares the same methodology of *AL*-index and basing on the SuperMAG data [Gjerloev, 2012].

3. Initial phase of the magnetic storm on 20 April 2020

The storm initial phase started at 02:30 UT when the solar wind density and dynamic pressure increased significantly, from 5 to 50 cm⁻³ and from 1.5 to 15 nPa correspondingly as it can be seen in Figure 2 and Figure 3a. However, the solar wind speed remained low at $V \sim 350$ km/s, and the B_z and B_y components of the IMF varied slightly.

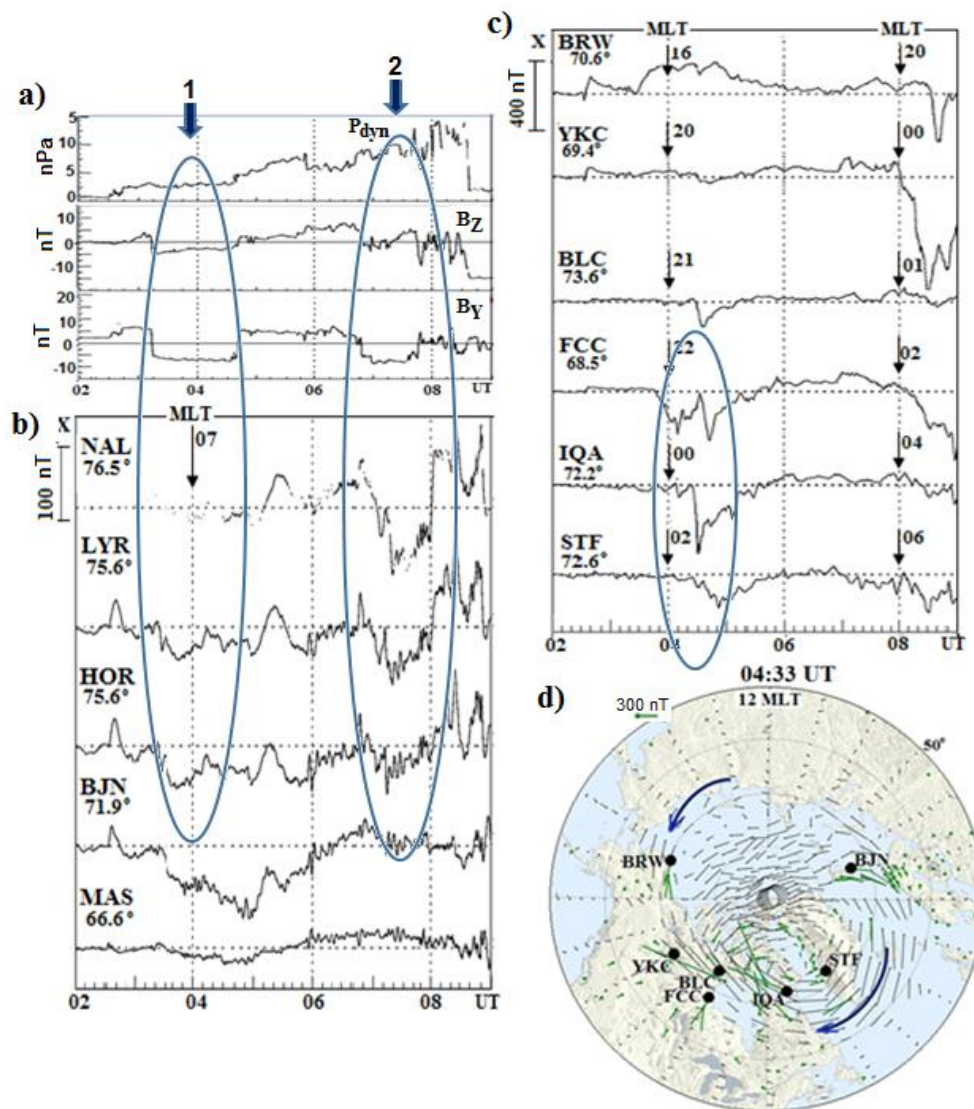


Figure 3. Initial phase of the storm: a) the solar wind pressure and the IMF B_z and B_y variations; (b) IMAGE stations located in the morning-daytime sector; (c) the same from the high latitude American stations located in the nighttime sector; (d) the instantaneous (at the maximum of the magnetic bay-1 at 04:33 UT) map of the magnetic vectors from ground-based SuperMAG magnetometers. Vectors of the magnetic field were rotated 90° clockwise to indicate ionospheric equivalent current direction. Blue arrows show maximum of the bays under consideration. Data from <http://omniweb.gsfc.nasa.gov>, <http://space.fmi.fi/image/> and <http://supermag.jhuapl.edu/mag>.

In Figure 3b one can see the negative bay-like geomagnetic disturbances in the morning and early-daytime sectors at the high-latitudes IMAGE stations. The IMF B_y was dominant, so, it

controlled the sign of the magnetic bays which agrees with previous results [e.g., Gromova et al., 2016].

Note, the magnetic bay-1, pointed by vertical line (1) in Figure 2, was more intense at HOR and LYR stations, but the magnetic bay-2 was more intense at the higher latitudes, at LYR and NAL stations. In the case of the substorm-2, the solar wind dynamic pressure was almost 2 times higher than during the substorm-1. The shift of the magnetic bay-2 to higher latitudes may be the result of the daytime polar cusp expansion with increasing the solar wind dynamic pressure.

The SuperMAG map of the magnetic vector distribution, built in the substorm maximum, shows two large-scale magnetic field vortices with centers in the post-midnight and afternoon sectors marked by the black arrows. They could be as an indicator of the local increase of the Field-Aligned Currents (FAC) under the low and unchanged solar wind speed.

3. Main phase of the storm

The main phase of the storm was associated with approach the Earth of the magnetic cloud with the large IMF B_T (up to 15 nT) and with southward turn of the IMF B_z . The sign of the SYM/H variations changed from positive to negative. At the same time the dynamic pressure of the solar wind dropped sharply but the solar wind speed remained low, $\sim 350\text{--}380$ km/s.

Geoeffectiveness of the magnetic cloud expressed in the development of two intense (more than 1000 nT) magnetospheric substorms observed in the main phase of the storm. They are pointed by the vertical lines (2) and (3) in Figure 2.

The scenario of these substorms is similar to the scenario of supersubstorm developed during a large storm main phase [Despirak et al., 2021]. On the SuperMAG map, presented in Figure 4c, one can see the substorm-1 ionospheric currents expanding from the evening to early morning sector (Figure 3d), and the substorm-2 currents expanding from the local midnight to almost 08 MLT. The centers of the electrojets were observed in the near-midnight sector, (Figure 4b) at latitudes below 65° MLAT, as it is indicated by positive deviations of the Z -component of the magnetic field in BRW and in CMO.

We could assume that these substorms were caused by the appearance of large amplitudes of the southward IMF B_z .

4. Conclusion

The magnetic storm on 20 April 2020 caused by a *slow* magnetic cloud approached the magnetosphere of the Earth was first moderate magnetic storm of the new 25 solar cycle. Despite of the low solar wind speed, geomagnetic disturbances during this storm were significant ($K_p = 5$).

- In the initial phase of the storm was developed under SHEATH conditions. There it was found two high-latitude magnetic field vortices with centers in the post-midnight and afternoon sectors. These vortices could be an indicator of the local enhancement of the Field Aligned Currents in the polar latitudes.
- We found that in the initial phase of this magnetic storm, the intensification of the FACs was observed under low values of the solar wind speed.
- In the main phase of the magnetic storm, associated with approach the Earth of the MC with the large IMF B_T there were two intense magnetospheric substorms observed. Apparently, they caused by the appearance of large amplitudes of the southward IMF B_z .

Thus, the first magnetic storm in the new solar activity cycle, despite the low speed of the solar wind, led to the development of the significant geomagnetic activity due to large negative values of the IMF B_z in the main phase of this storm. We conclude that the geoeffectiveness of this magnetic storm depended more on the appearance of large values of the southward IMF than on the low values of the solar wind speed.

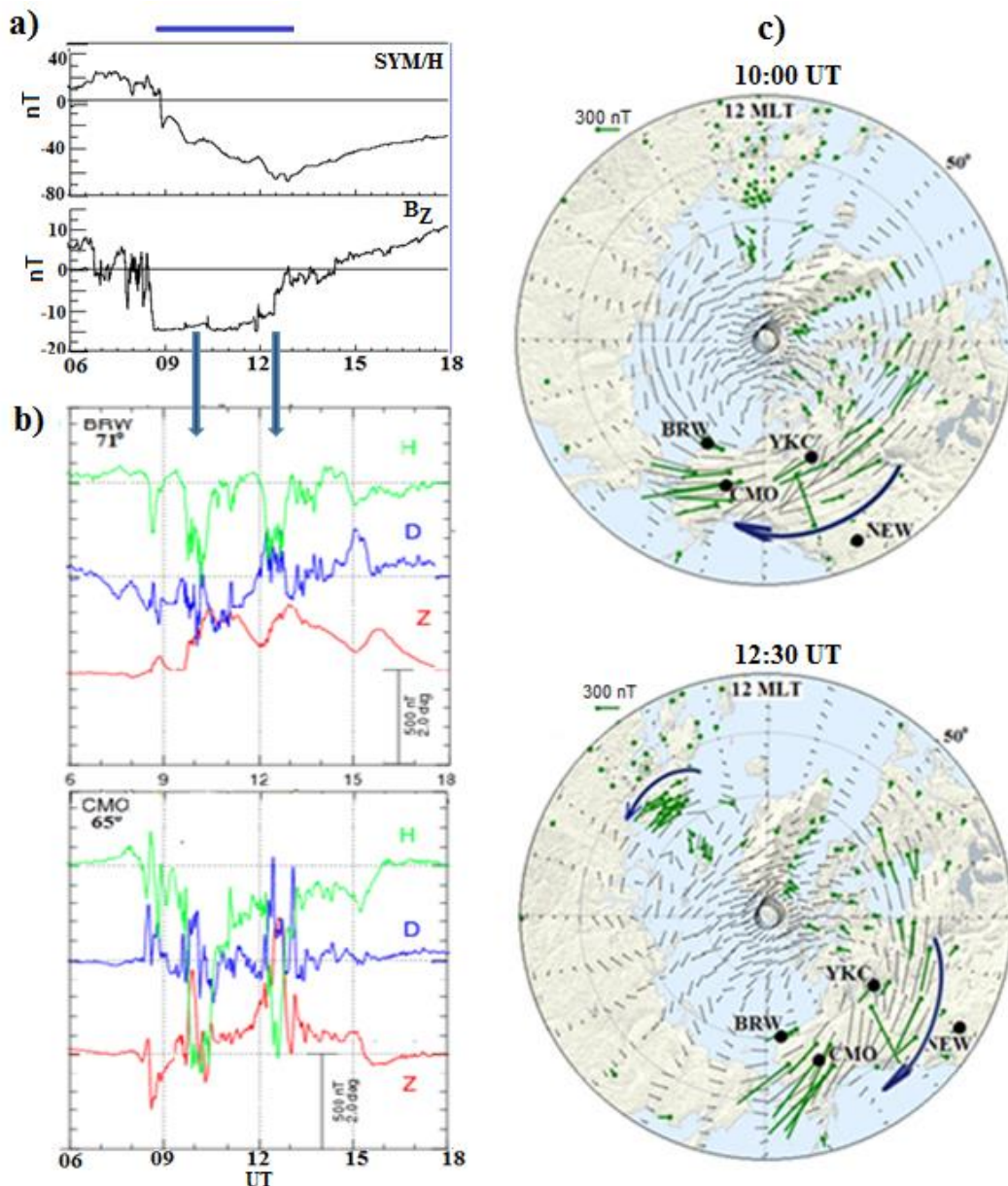


Figure 4. Interplanetary conditions and variations of the geomagnetic field in the main phase of the storm: (a) SYM/H-index and the IMF Bz; b) H-, D-, Z-components of the geomagnetic field at BRW and CMO stations (data from https://wdc.kugi.kyoto-u.ac.jp/plot_realtime/qu); c) the instantaneous map of the magnetic field vectors from ground-based SuperMAG magnetometers in the maximum of substorms under consideration, pointed by the blue arrows.

Acknowledgments

The authors are grateful to the creators of OMNI (<http://omniweb.gsfc.nasa.gov>), SuperMAG (<http://supermag.jhuapl.edu>), IMAGE (<http://space.fmi.fi/image/>), Intermagnet (<https://www.intermagnet.org/>), World Data Center for Geomagnetism, Kyoto (https://wdc.kugi.kyoto-u.ac.jp/plot_realtime) for allowing to use these databases in our study.

References

Davies, E.E., Möstl, C., Owens, M.J. et al. (2021). In situ multi-spacecraft and remote imaging observations of the first CME detected by Solar Orbiter and BepiColombo, A&A, V 656, id. A2. <https://doi.org/10.1051/0004-6361/202040113>

- Despirak, I.V., Lyubchich, A.A., Kleimenova, N.G. *et al.* (2021). Longitude Geomagnetic Effects of the Supersubstorms during the Magnetic Storm of March 9, 2012. *Bull. Russ. Acad. Sci. Phys.*, (2021). V 85, pp.246–251. <https://doi.org/10.3103/S1062873821030096>
- Gjerloev J.W. (2012). The SuperMAG data processing technique, *J. Geophys. Res.*, V 117, A09213. <https://doi.org/10.1029/2012JA017683>
- Gromova, L.I., Kleimenova, N.G., Gromov, S.V., Dremukhina, L.A., and Zelinskii, N.R., Daytime geomagnetic disturbances at high latitudes during a strong magnetic storm of June 21–23, 2015: The storm initial phase, *Geomagn. Aeron. (Engl. Transl.)*, 2016, V 56, No. 3, pp. 281–292.
- Kliemenova, N.G., Gromova, L.I., Gromov, S.V. *et al.* (2021). High-Latitude geomagnetic disturbances and field-aligned currents in the recovery phase of the large magnetic storm, *Geomagn. Aeronom.* V 61, No 4, pp. 520-528. <https://doi.org/10.31857/S0016794021040076>
- Nitta, N.V., Mulligan, T., Kilpua, E.K. (2021). Understanding the origins of problem geomagnetic storms associated with “Stealth” coronal mass ejections, *Space Sci. Rev.*, V 217, id. 82. <https://doi.org/10.1007/s11214-021-00857-0>
- O’Kane, J., Green, L. *Davies E.*, *et al.* (2021). Solar origins of a strong stealth CME detected by Solar Orbiter, *A & A*, V 656, id. L6. <https://doi.org/10.1051/0004-6361/202140622>
- Richardson, I.G., Cane H. V. (2012). Solar wind drivers of geomagnetic storms during more than four solar cycle. *J. Space Weather Space Clim.*, V. 2, A01. <https://doi.org/10.1051/swsc/2012001>
- Tsurutani, B.T., Gonzalez W.D., Tang F. *et al.* (1992). Great magnetic storms, *Geophys. Res. Lett.* V. 9. – pp. 73-76. <https://doi.org/10.1029/91GL02783>